

ORIGINAL RESEARCH ARTICLE

A study of electrocatalytic ethanol oxidation of nanoporous PtSi alloy

Nali Lu^{1,3}, Yao Li^{2,3}, Lei Zhang^{3,4}, Yong Fang^{3,4}, Bin Qian^{3,4}, Zhida Han^{3,4*}, Xuefan Jiang^{3,4}

¹ School of Materials Science and Engineering, China University of Mining and Technology, Xuzhou 221116, China

² College of Chemistry, Chemical Engineering and Materials Science, Soochow University, Suzhou 215123, China

³ School of Physics and Electronic Engineering, Changshu Institute of Technology, Changshu 215500, China. E-mail: han@cslg.edu.cn

⁴ Jiangsu Key Laboratory of Advanced Functional Materials, Changshu 215500, China

ABSTRACT

In recent years, nanoporous alloys have presented the advantages of a large specific surface area, low density, and simple operation, and they have been widely used in the fields of catalysis, magnetism, and medicine. Nanoporous Pt-Si alloy was prepared by melt-spun and chemical dealloying, and was characterized by X-ray diffraction, X-ray photoelectron spectroscopy, scanning electron microscope, and transmission electron microscopy. Pt-Si alloys possess a three-dimensional bicontinuous structure and an average size of 5 nanometers. Compared with commercial Pt/C catalysts, nanoporous Pt-Si alloys exhibit excellent electrocatalytic activity and stability in ethanol-catalyzed oxidation reactions. It is taken into consideration to be a promising catalyst in direct ethanol fuel cells.

Keywords: Dealloying; Nanoporous; Electrocatalysis; Ethanol Oxidation Reaction

ARTICLE INFO

Received: 14 December 2020

Accepted: 3 February 2021

Available online: 10 February 2021

COPYRIGHT

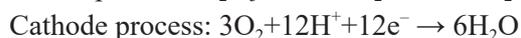
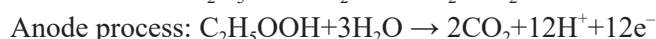
Copyright © 2021 Nali Lu, *et al.*

EnPress Publisher LLC. This work is licensed under the Creative Commons Attribution-NonCommercial 4.0 International License (CC BY-NC 4.0).

<https://creativecommons.org/licenses/by-nc/4.0/>

1. Introduction

The fuel cell is an energy conversion device, which can directly convert the energy generated by fuel through chemical reactions into electric energy, and only water is generated in the entire process^[1]. A fuel cell combines the best characteristics of an internal combustion engine and battery, like an internal combustion engine that can run only with fuel without any mechanical conversion process. Fuel cells are similar to those under load conditions^[2]. Direct ethanol fuel cell (DEFC) uses ethanol as fuel, which has attracted more and more attention. Ethanol, as a small alcohol organic molecule, converts the chemical energy into electrical energy, has higher capacity density, low toxicity, and is convenient for storage and transportation, as well as the advantages of large-scale preparation of biomass products, it is widely used in mobile devices such as automobiles, mobile phones and computers^[3-5]. The research of Wang *et al.*^[6] shows that the permeability of ethanol through the electrolytic membrane is lower than that of methanol. Under acidic conditions, the reaction process of ethanol is as follows:



The reaction mechanism of ethanol is very complex, involving 12 e transfers, accompanied by the fracture of the C–C bond, the interme-

diate products dominated by COads are generated, which gather on the surface of the catalyst and produce poisoning phenomenon that reduces the activity of the catalyst. In practical application, the catalytic oxidation of ethanol requires a high overpotential. Therefore, developing new anode catalysts with high activity and high stability has become a research hotspot. The existing research shows that the improvement of the performance of Pt-based catalysts is due to the shortening of Pt metal bonds, the enhancement of bond energy, and the easier adsorption of oxygen after alloying; the microstructure between materials is changed, the alloying effect of different elements, the specific surface area increases, and the active sites increase. To mix Pt with other non-noble metals^[7-9], and the microstructure of Pt is optimized to prepare nano Pt catalyst with controllable morphology^[10], which can prevent the aggregation of Pt particles due to the synergistic effect between bimetallic metals and is helpful to improve the stability of the catalyst^[11,12].

Based on the different properties of different elements, the dealloying method uses chemical or electrochemical methods^[13] to remove the more active components in the alloy. Then the remaining components finally obtain more stable elements through diffusion and aggregation to form the framework of nanometal materials^[13-15]. In recent years, Chen *et al.*^[16] proposed a reverse dealloying method to prepare nanosilver. To selective remove the inert component Au in Au-Ag alloy. Meanwhile, thiourea plays a role in promoting gold dissolution and passivating silver in the process of forming the porous silver framework^[16]. According to Liu *et al.*^[17], by changing the time sequence of dealloying, a series of nanoporous metal compound products with bimodal porous metals and single peak pores can be synthesized^[17]. At present, Pt and 3d transition metals M (such as Ti, Cr, V, Mn, Fe, Co, Ni, Cu^[18-20]) form alloys and are loaded on carbon carrier, which can effectively improve the stability of catalysts. Relevant literature reports Pt-Sn^[21], Pt-W^[22], and other alloy catalysts also show CO tolerance and are excellent catalysts^[21,22]. Considering the small radius of the Si atom, the introduction of the Si atom reduces the

distance between Pt-Pt and enhances the catalytic activity. In addition, Si is relatively stable under acidic conditions and can obtain better stability. Therefore, that alloying Pt and Si expects to improve the electrocatalytic performance of the material. Although studies have shown that bulk Pt-Si alloy^[23] has great electrocatalytic oxidation activity for methanol and carbon monoxide, nano-scale Pt-Si alloy and its catalytic performance have not been reported^[23].

In this study, we successfully prepared a 3D framework nanoporous PtSi (NP PtSi) binary alloy through the combination of melt rapid quenching technology and dealloying. Meanwhile, it also studied its electrocatalytic oxidation activity and stability for ethanol.

2. Experiment

2.1 Sample preparation

The purity of metal materials Pt, Si and Al is more than 99.99%, and the corresponding stoichiometric ratio is 9:3:88. Then calculate their respective elemental mass. Put the prepared materials into a water-cooled copper crucible electric arc furnace, and inject Ar gas to melt repeatedly 3–4 times to obtain Pt₉Si₃Al₈₈ alloy ingot. Cut the melted Pt₉Si₃Al₈₈ alloy ingot into small pieces, put it into the fired quartz glass tube and melt the material slowly to obtain the alloy strip with basically the same thickness. Weigh about 50 mg of the strip and put it in 5 wt% HCl solution to produce lots of bubbles at the beginning. When the reaction is slow, put it into a constant temperature water bath at 50 °C Celsius for 48 h, take out the sample, centrifuge and wash it repeatedly 5–6 times. Finally, it obtains the NP-PtSi by drying in a vacuum drying oven for 24 h.

2.2 Characterization of materials

We used the SA-HF3 X-ray powder diffractometer (XRD) of Rigaku Company from Japan to analyze the crystal structure of the materials. Detecting the chemical composition and surface atomic state of the material by the X-ray photoelectron spectroscopy (XPS) of Axis Ultra, which is a wholly-owned subsidiary of Shimadzu group in Japan. The Sigma

scanning electron microscope (SEM) of ZEISS Company in Germany was used to observe the micromorphology of the material, the accelerating voltage is 20 kV. TecnaiG220S-TWIN transmission electron microscope (TEM) and high-resolution transmission electron microscope (HRTEM) of American FEI Company are used, which not only could detect the microstructure of materials but also obtain the crystal plane spacing of atoms. The electrochemical properties of materials are measured by the electrochemical workstation of model 760E of Shanghai Chenhua Instrument Co., Ltd.

2.3 Electrode preparation and electrochemical test

Weigh 1 mg of NP-PtSi and 1.5 mg of carbon black with an electronic balance into a 2 ml centrifuge tube, and put 980 μL absolute ethanol and 20 μL 5 wt% Nafion with a pipette gun respectively into a centrifuge tube. Then put into an ultrasonic cleaner for about 1h to obtain the catalyst suspension. Commercial Pt/C catalyst with the same concentration was prepared by the same method.

Firstly, the glassy carbon electrode (GCE, diameter 3 mm) was applied on the foot skin with 0.05 μm polishing powder shall be polished and cleaned with ultrapure water, and then placed in the mixed solution of 0.1 mol/L KCl + 1 mol/L potassium ferricyanide to measure the redox potential difference. When the value is less than 70 mV, it shall be washed with ultrapure water and dry naturally for standby.

All electrochemical tests were carried out in a three-electrode system. Before the reaction, introducing saturated N_2 , removing O_2 from the solution, and the reaction temperature was 25 degrees Celsius.

3. Results and discussion

3.1 Characterization of NP-PtSi

3.1.1 XRD characterization of NP-PtSi

Figure 1 is the XRD diagram of $\text{Pt}_9\text{Si}_3\text{Al}_{88}$ alloy before and after dealloying. It shows from the diagram that the diffraction peak of PtSiAl alloy is

very complex, and it is difficult to distinguish the alloy phase of PtSiAl, and there is no diffraction peak corresponding to pure Pt, Al, and Si, indicating the formation of Pt-Si alloy. NP-PtSi sample has three diffraction peaks, i.e. $2\theta = 40.140^\circ$, 46.599° , and 68.317° , corresponding to (111), (200), (220) crystal planes of face-centered cubic PtSi. Compared with the standard pure Pt card (JCPDS 04-0802), it finds that the diffraction peak of each crystal plane deviates slightly to a high angle, which may be because Si atoms with small atomic radius are added into the alloy to replace some Pt atoms, which reduces the distance between Pt-Pt and finally forms Pt-Si alloy.

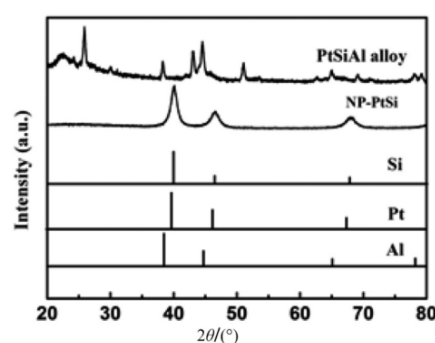


Figure 1. XRD spectra of $\text{Pt}_9\text{Si}_3\text{Al}_{88}$ alloy before and after dealloying. Standard spectra: Pt (JCPDS04-0802), Si (JCPDS35-1158), Al (JCPDS 04-0787).

3.1.2 XPS characterization of NP-PtSi

Figure 2(a) is the full spectrum of NP-PtSi. By that, we can see the peaks of Pt 4f, Si 2f, O 1s, C 1s, and other elements, in which O 1s and C 1s belong to water or carbon dioxide physically or chemically adsorbed on the material surface, which fits with XPS Peak Fit^[13]. **Figure 2(b)** is the peak diagram of Pt 4f. There are two peaks at 71.2 eV and 74.6 eV, corresponding to Pt and Pt^{2+} in the metal state. The results show that some Pt is oxidized to Pt^{2+} , but it mainly exists in the form of Pt in a metal state, which is consistent with the internal XRD test results of the material. **Figure 2(c)** is the sub-peak diagram of Si 2p. Both Si^0 and Si^{4+} can be detected, and the binding energy belongs to Si^0 at 99.5 eV; the binding energy belongs to Si^{4+} at 103.2 eV. On the surface, Si mainly exists in the form of Si^{4+} . It also can observe some metallic Si.

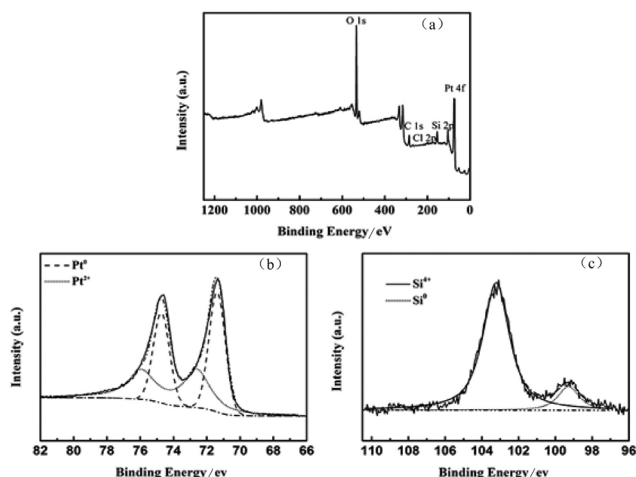


Figure 2. (a) XPS full spectrum of NP-PtSi; (b) Pt 4f peak diagram; (c) Si 2p peak diagram.

3.1.3 SEM, TEM and HRTEM characterization of NP PtSi

Figure 3(a) is the SEM diagram of $\text{Pt}_9\text{Si}_3\text{Al}_{88}$ strip after dealloying, which shows that it forms a uniform nanoporous structure composed of nanopores and ligaments. The pore size is 5–20 nm, the specific surface area increases, and the active sites of an electrochemical reaction in the material increase. **Figure 3(b)** is the cross-sectional view of NP-PtSi, from which the uniform pores can be seen. This confirms that the fine nanoporous structure is obtained in the whole sample. The TEM diagram can observe the microstructure of the sample from the nano size, as shown in **Figure 3(c)**. The uniformly distributed bright white areas can be seen more clearly from the TEM diagram. Compared with the SEM diagram, the structure with pores in the multi-level pores is more significant. It is conducive to improving the kinetics of oxygen diffusion. **Figure 3(d)** is the HRTEM diagram of NP-PtSi, and it is clear that

the continuous lattice diffraction fringes.

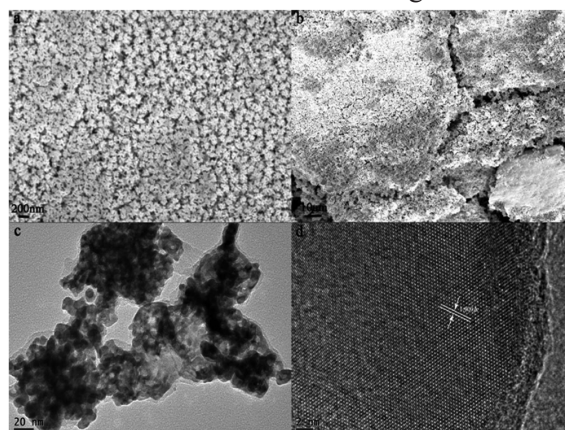


Figure 3. Characterization diagram of NP-PtSi alloy. (a) SEM diagram; (b) SEM diagram; (c) TEM diagram; (d) HRTEM diagram.

3.2 Electrochemical performance test of NP-PtSi

In 0.5 mol/L H_2SO_4 deoxidized solution, the stable CV curve of NP-PtSi alloy is shown in **Figure 4 (a)**, and commercial Pt/C catalysts can be compared. In the whole potential scanning range, NP-PtSi and commercial Pt/C catalysts show the same CV curve characteristics, including hydrogen adsorption and desorption zone: $-0.25\text{--}0.1$ V vs. SCE; electric double layer area: $0.1\text{--}0.35$ V vs. SCE; high potential region: $0.35\text{--}1.2$ V vs. SCE. In the hydrogen adsorption and desorption region, the peak of NP-PtSi alloy becomes wider and shifts to high potential compared with commercial Pt/C, which is due to the increase of hydrogen adsorption strength on Pt due to the interaction between Pt and Si. Compared with commercial Pt/C catalyst, NP-PtSi shows a significant current peak at about 0.45 V vs. SCE, which shows that lots of OH species adsorb on the surface of the catalyst.

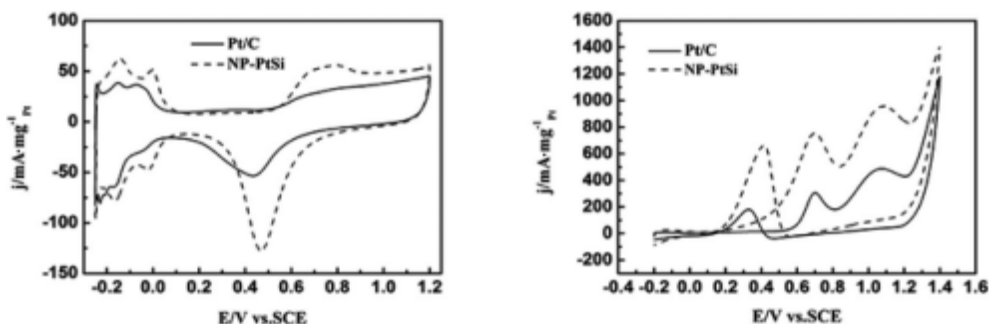


Figure 4. Cyclic voltammetric curves of Pt/C and NP PtSi catalysts in deaeration solution. (a) 0.5 mol/L H_2SO_4 solution; (b) 0.5 mol/L H_2SO_4 + 1 mol/L $\text{CH}_3\text{CH}_2\text{OH}$ mixed solution.

It believes that the activity of the catalyst is related to the electrochemical activity area (ECSA). We use Origin software to calculate the desorption peak area of H, and the formula is $ECSA = QH/(m \times c)$. In the formula, Q is the Coulomb charge $mC \cdot cm^{-2}$ in the H region, m is the Pt load, $mg \cdot cm^{-2}$, and c is the charge density adsorbed by the monolayer of H of Pt, which is $0.210 mC \cdot cm^{-2}$. It shows in **Figure 4(a)** that the electrochemically active area of NP-PtSi is much larger than that of commercial Pt/C, indicating that the number of active sites of NP-PtSi catalyst after dealloying is increased, which is conducive to the catalytic oxidation of ethanol.

Figure 4(b) shows the CV curve of NP-PtSi and commercial Pt/C catalyst in the mixed solution of $0.5 \text{ mol/L H}_2\text{SO}_4 + 1 \text{ mol/L CH}_3\text{CH}_2\text{OH}$. During the potential positive scanning, there are two oxidation peaks. During the negative scanning, there is a reduction peak. The Pt-based catalyst surface will adsorb -OH and be oxidized to PtO. During the negative scanning, PtO is restored. The oxidation peak (I) is about 0.7 V , which is usually taken into consideration as the characteristic peak of ethanol oxidation to CO_2 . It is one of the basis for judging the performance of the catalyst. The oxidation peak (II) is about 1.1 V , which is related to the secondary oxidation of intermediate products. The peak onset potential is also a key index for evaluating the activity of the catalyst. The peak onset potential of NP-PtSi alloy is negative compared with that of commercial Pt/C catalyst, which shows that the catalyst can improve the catalytic oxidation kinetics of ethanol and has good application value.

We further explored the stability of NP-PtSi alloy and commercial Pt/C catalyst by the potentiostat method. **Figure 5** is the I-t curve with a constant potential of 0.7 V . It shows from the figure that at the beginning, the current density of NP-PtSi and Pt/C catalyst decreased sharply due to the formation of electric double-layer capacitance. The subsequent decrease in current is due to the loss of surface activity sites caused by the adsorption of oxygen-containing intermediate species on the catalyst surface. After 500 s , the current density tends to be stable, which attributes to the continuous reduction of cat-

alyst concentration during the reaction. Although the current density of both decreased to varying degrees within the entire $3,000 \text{ s}$, the current density of NP-PtSi is always higher than that of commercial Pt/C catalyst, indicating that the addition of Si makes NP-PtSi alloy show better stability than commercial Pt/C catalyst.

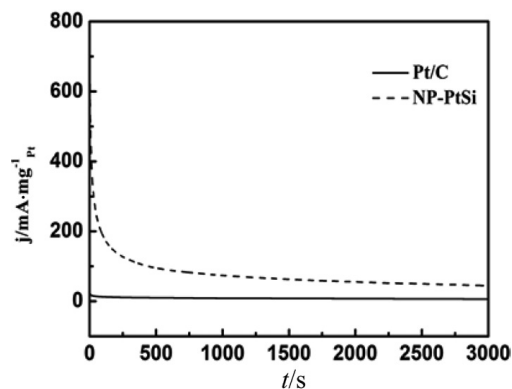


Figure 5. Potentiostatic I-t curve of Pt/C and NP-PtSi catalysts in mixed solution of $0.5 \text{ mol/L H}_2\text{SO}_4 + 1 \text{ mol/L CH}_3\text{CH}_2\text{OH}$ (constant potential is 0.7 V).

4. Conclusion

Nanoporous Pt-Si alloy was prepared by the combination of melt rapid quenching technology and dealloying. NP-PtSi alloy has a three-dimensional bi-continuous structure, with an average pore size of 5 nm and a large specific surface area. Compared with commercial Pt/C catalyst, NP-PtSi alloy has excellent ethanol electrocatalytic activity and stability under acidic conditions, and the operation is simple, the conditions are easy to control, the cost is low, and it can produce on a large scale, which makes NP-PtSi alloy have more application potential in the field of electrocatalysis.

Conflict of interest

The authors declare that they have no conflict of interest.

Acknowledgements

Project: the National Natural Science Foundation of China Project “Research on low temperature phase effect of phase separation and exchange biasing of alloy of Ni-Mn based magnetic shape memory alloy” (51371004).

References

1. Hou M, Yi B. Development status of fuel cell technology (in Chinese). *Chinese Journal of Power Sources* 2008; (10): 649–654.
2. Cook B. Introduction to fuel cells and hydrogen technology. *Engineering Science and Education Journal* 2002; 11(6): 205–216.
3. Qu Y, Wang L, Li C, *et al.* Quantitative pinhole online electrochemical mass spectrometry study on ethanol electro-oxidation at carbon-supported Pt and Ir-containing catalysts. *International Journal of Hydrogen Energy* 2017; 42(1): 228–235.
4. Yang W, Lu M, He Y. Performance study of an alkaline direct ethanol fuel cell with a reduced two-dimensional mass transport model. *International Journal of Hydrogen Energy* 2016; 41(45): 20693–20708.
5. Abrego-Martinez JC, Wang Y, Mendoza-Huizar LH, *et al.* Mixed-reactant ethanol fuel cell using an electrochemically deposited Ag@Pt tolerant cathode. *International Journal of Hydrogen Energy* 2016; 41(48): 23417–23424.
6. Wang J, Wasmus S, Savinell RF. Evaluation of ethanol, 1-propanol, and 2-propanol in a direct oxidation polymer-electrolyte fuel cell. *Journal of the Electrochemical Society* 1995; 142: 4218–4224.
7. Koh S, Strasser P. Electrocatalysis on bimetallic surfaces: Modifying catalytic reactivity for oxygen reduction by voltammetric surface dealloying. *Journal of the American Chemical Society* 2007; 129(42): 12624–12625.
8. Kattel S, Wang G, Duan Z. Density functional theory study of oxygen reduction reaction mechanism on Pt alloy catalysts. *Journal of Physical Chemistry C* 2014; 1: 911.
9. Wang C, Vliet DVD, More K, *et al.* Multimetallic Au/FePt₃ nanoparticles as highly durable electrocatalyst. *Nano Letters* 2010; 11(3): 919–926.
10. Jiang L, Sun G, Sun S, *et al.* Structure and chemical composition of supported Pt-Sn electrocatalysts for ethanol oxidation. *Electrochimica Acta* 2005; 50(27): 5384–5389.
11. Yu X, Ye S. Recent advances in activity and durability enhancement of Pt/C catalytic cathode in PEMFC. *Journal of Power Sources* 2007; 172(1): 145–154.
12. Luo Y, Liang Z, Liao S. Recent development of anode electrocatalysts for direct methanol fuel cells. *Chinese Journal of Catalysis* 2010; 31(2): 141–149.
13. Senior NA, Newman R. Synthesis of tough nanoporous metals by controlled electrolytic dealloying. *Nanotechnology* 2006; 17(9): 2311–2316.
14. Stratmann M, Rohwerder M. A pore view of corrosion. *Nature* 2001; 410: 421–423.
15. Erlebacher J. An atomistic description of dealloying-porosity evolution, the critical potential, and rate-limiting behavior. *Journal of the Electrochemical Society* 2004; 151(10): C614–C626.
16. Chen T, Liu Z, Lu W, *et al.* Fabrication of free-standing nanoporous silver by selectively dissolving gold from gold-silver alloys via a novel inverse dealloying method. *Electrochemistry Communications* 2011; 13(10): 1086–1089.
17. Liu W, Zhang S, Li N, *et al.* A general dealloying strategy to nanoporous intermetallics, nanoporous metals with bimodal, and unimodal pore size distributions. *Corrosion Science* 2012; 58(5): 133–138.
18. Kattel S, Duan Z, Wang G. Density functional theory study of an oxygen reduction reaction on a Pt₃Ti alloy electrocatalyst. *Journal of Physical Chemistry C* 2013; 117(14): 7107–7113.
19. Ohyagi S, Sasaki T. Durability of a PEMFC Pt-Co cathode catalyst layer during voltage cycling tests under supersaturated humidity conditions. *Electrochimica Acta* 2013; 102(15): 336–341.
20. Hoffmannová H, Okube M, Petrykin V, *et al.* Surface stability of Pt₃Ni nanoparticulate alloy electrocatalysts in hydrogen adsorption. *Langmuir* 2013; 29(29): 9046–9050.
21. Liu Z, Jackson GS, Eichhorn BW. PtSn intermetallic, core-shell, and alloy nanoparticles as co-tolerant electrocatalysts for H₂ oxidation. *Angewandte Chemie International Edition* 2010; 49(18): 3173–3176.
22. Pereira LGS, Paganin VA, Ticianelli EA. Investigation of the CO tolerance mechanism at several Pt-based bimetallic anode electrocatalysts in a PEM fuel cell. *Electrochim Acta* 2009; 54(7): 1992–1998.
23. Rohner A, Han B, Jensen JO, *et al.* Pt-Si bifunctional surfaces for CO and methanol electro-oxidation. *Journal of Physical Chemistry C* 2015; 119(15): 8023–8031.